Molecular basis of class III ligand recognition by PDZ3 in murine protein tyrosine phosphatase PTPN13

[1]Gerd Kock, [1]Markus Dicks, [1]King Tuo Yip, [1]Bastian Kohl, [1]Stefanie Pütz, [2]Rolf Heumann, [3]Kai S. Erdmann, and [1]Raphael Stoll[*]

[1]Biomolecular NMR Spectroscopy, Faculty of Chemistry and Biochemistry, Ruhr-University of Bochum, D-44780, Germany

[2]Biochemistry II, Faculty of Chemistry and Biochemistry, Ruhr-University of Bochum, D-44780, Germany

[3]Department of Biomedical Science, University of Sheffield, Sheffield S10 2TN, United Kingdom

[*]To whom correspondence should be addressed:

Raphael Stoll

Ruhr University of Bochum

Faculty of Chemistry and Biochemistry

Biomolecular NMR Spectroscopy

44780 Bochum

Germany

Tel.: +49 234 32 25466

Fax: +49 234 32 05466

E-mail: raphael.stoll@ruhr-uni-bochum.de

Key words

PTPN13, PDZ3, PRK2, PDZ ligand class I and III, complex, structure in solution, NMR spectroscopy

Character count: 65,720 **(**including spaces)

Abstract

Protein tyrosine phosphatase PTPN13, also known as PTP-BL in mice, represents a large multi domain non-transmembrane scaffolding protein that contains five consecutive PDZ domains. Here, we report the solution structures of the extended murine PTPN13 PDZ3 domain in its apo form and in complex with its physiological ligand, the carboxy-terminus of PRK2, determined by multidimensional NMR spectroscopy. Both in its ligand-free state and when complexed to PRK2, PDZ3 of PTPN13 adopts the classical compact, globular D/E fold. PDZ3 of PTPN13 binds five carboxy-terminal amino acids of PRK2 *via* a groove located between the EB-strand and the DB-helix. The PRK2 peptide resides the canonical PDZ3 binding cleft in an elongated manner and the amino acid side chains in position P0 and P-2, cysteine and aspartate, of the ligand face the groove between EB-strand and DB-helix, whereas the PRK2 side chains of tryptophan and alanine located in position P-1 and P-3 point away from the binding. These structures are rare examples of selective class III ligand recognition by a PDZ domain and now provide a basis for the detailed structural investigation of the promiscuous interaction between the PDZ domains of PTPN13 and of their interaction with ligands. They will also lead to a better understanding of the proposed scaffolding function of these domains in multi-protein complexes assembled by PTPN13 and could ultimately contribute to low molecular weight antagonists that could even act on the protein kinase C-related kinase-2 (PRK2) signalling pathway to modulate rearrangements of the actin cytoskeleton.

Introduction

The protein tyrosine phosphatase PTPN13 and its mouse homologue, PTP-basophil-like (PTP-BL), are high molecular non-transmembraneous protein phosphatases that contain various protein-protein interaction modules. The amino-terminal part of murine PTPN13 (UNIPROT Q64512) consists of a KIND (kinase non-catalytic C-lobe; residues 3-190) domain, followed by a FERM (Four point one, Ezrin, Radixin, Moesin; residues 565-865) domain that is involved in the association of proteins to the plasma membrane. In addition, PTPN13 contains five PDZ domains (PDZ1: residues 1084-1170; PDZ2: residues 1357-1442; PDZ3: residues 1491-1579; PDZ4: residues 1764-1845; PDZ5: residues 1857-1942) as well as a carboxy-terminal protein tyrosine phosphatase domain (residues 2180-2434) [1]. While structures of PDZ2b of PTPN13 and PDZ2 of PTPN13 have been solved, the structure of the PDZ3 domain still remained elusive to date [2], [3]. PDZ domains share a globular fold that consists of two α-helices (DA and DB) and 6 β-strands (EA to EF), which form two anti-parallel β-sheets [4], [5]. PDZ domains are well-known to mediate protein-protein interactions and are crucial for the assembly of a number of multiprotein complexes [6]. Currently, a large number of PTPN13 interacting proteins are already known and it is of great interest to further characterise binding properties of the PDZ domain module located in PTPN13. For example, it was shown that PDZ1 of PTPN13 binds to IκBα [7], [8], [9]. In addition, only one of the two splicing variants of PDZ2 interacts with the tumour suppressor protein APC (adenomatous polyposis coli), whereas PDZ3 associates with the protein kinase PRK2 [1], [27]. It is also known that one of the proteins that interacts with PDZ4 of PTPN13 is CRIP2, a LIM-only protein (for a review see [1]. PDZ domains 2, 3, and 5 are also capable of binding the phospholipid

phosphatidylinositol-4,5-bisphosphate [10]. Interestingly, PTPN13 is not the only protein that contains multiple PDZ domains. For instance, the membrane-associated guanylate kinase (MAGUK) family of proteins carries several, mostly class I PDZ domains in addition to other protein binding modules, such as SH3 and WW domains [11], [12]. Like PTPN13, MAGUK proteins serve as scaffolding proteins that associate to transmembrane tight-junction-associated proteins, the cytoskeleton, and signal transduction molecules [12]. MAGUK proteins use a combination of several modular domains that yield complex scaffolding functions at different subcellular, cellular, and even systems level [11]. Apparently, cooperative effects in multi-domain PDZ proteins modulate their affinity towards ligands bearing a PDZ-ligand binding motif (PBM).

PDZ domains serve as interaction modules that gather functionally distinct proteins in order to form multifunctional supramolecular complexes. Therefore, PDZ (PSD-95, discs large, *Zonula occludens*) domain-containing proteins are frequently denoted as scaffolding proteins that selectively bind to the carboxy-termini of their protein targets. PSD95, for instance, is a membrane-associated member of the guanylate kinase family of proteins that binds to neuronal glutamate receptors to form a macromolecular complex [13], [14]. The PDZ domain-containing proteins Afadin and ZO1 interact with the cytoskeleton and stabilise cells and tissue [15], [16]. To date, numerous structures of PDZ-ligand complexes have been solved either by NMR spectroscopy or X-ray crystallography providing fundamental insights into the molecular mechanisms of how PDZ domains recognise and stabilise their bound ligands [17]. PDZ domains are classified according to their binding specificity towards certain C-terminal binding motifs of their potential binding partners. A sequence alignment of 30 different PDZ classes clearly reveals

a high degree of amino acid residue conservation for the binding site and neighboring secondary structure elements, whereas the remaining regions are less conserved (Fig. 1). However, the interaction of the third PDZ domain of PTPN13 (PDZ3) with its natural ligand PRK2 presented here exhibits a novel mode of selectivity: In PRK2, the carboxyl-terminus is constituted by a cysteine residue that displays an unusual motif with respect to the hydrophobic binding pocket of most PDZ domains known so far [18]. This discovery reveals a new mechanism of ligand binding with fundamental implications for the unexpectedly high variability of PDZ domains to select and recognize their ligands.

Previously, several systems to categorise PDZ domains have been suggested in order to describe, decipher, and even predict their ligand selectivity. According to Nourry *et al.* [19], the PDZ3 domain of PTPN13 belongs to the modular class I-2 of PDZ proteins. This class contains PDZ proteins that lack intrinsic enzymatic activity and contain additional functional domains [19]. Bezprozvanny *et al.* [20] introduced a classification system of PDZ domains that is based on two crucial positions in their primary structure. On the one hand, the amino acid immediately following the EB β-sheet is denoted as position number 1. On the other hand, the first amino acid of the DB α-helix is defined as position number 2. According to this system, the PDZ3 domain of PTPN13 belongs to the rather small Sp,p group as it is the only PDZ domain that carries an R and a Q at these positions in its amino acid sequence. At the same time, Vaccaro *et al.* [18] introduced a different system that classifies PDZ domains according to the four terminal amino acids of their respective ligands. This yields four different, degenerated classes. PDZ domain class I recognises ligands that carry the sequence motif -X-S/T-X-Φ/Ψ-COOH (Φ=hydrophobic, Ψ=aromatic, X=any amino

acid). According to this system, class II PDZ domains bind to -X- Φ/Ψ-X- Φ/Ψ-COOH containing ligands, whereas class III PDZ proteins interact with a -X-D/E-X-Φ-COOH motif. Finally, members of class IV select PDZ ligands that contain a -X-X-Ψ-D/E-COOH motif [18]. Interestingly, the GLGF motif in class III PDZ domains is less conserved than in the other two classes, I and II (Fig. 1). This holds also true for the histidine residues at the beginning of the DB-α helix. Apparently, the rarely occurring class III PDZ domains exhibit a higher degree of ligand promiscuity. For example, the neuronal nitric oxide synthase (nNos) not only binds to class III ligands but also interacts with carboxy-terminal PDZ ligands of nNos (CAPON) as well as with other PDZ domains of PSD95 [21]. Proteins of the ALP/Enigma family, such as the PDZ and LIM domain containing protein 4 (RIL) or Zasp, bind to both class III and classical class I ligands, like the carboxy-terminus of D-Actinin-2 [22]. Afadin (AF-6), for instance, binds to classical class III ligands, such as c-Src, to class I, as well as to class II ligands [19, 23]. The PDZ1 domain of Mint1 not only binds to N-type Ca^{2+} channels, class III ligands, but also to Neurexin1D, a class I ligand [20]. Finally, the Syntenin PDZ1 domain interacts with the D chain of the Interleukin 5 receptor, a class I ligand, and with the *moesin-ezrin-radixin*like protein Merlin, a class III ligand [24]. The majority of PDZ domains identified so far belongs to class I, followed by members of class II. PDZ domains assigned to class III, however, are rare [23], [25]. According to this classification, the carboxy-terminal PRK2 peptide is a class III ligand, whereas APC peptide represents a class I ligand. It has been shown that PTPN13 is involved in the regulation of both cytoskeleton and intracellular vesicular transport [1], [26]. Protein kinase C-related kinase-2 (PRK2) – a serine/threonine kinase – serves as a potential effector target of both Rho and Rac GTPases that mediates their effects on rearrangements of the actin

cytoskeleton. Hence, the interaction of PTPN13 with PRK2 plays a physiologically important role. This interaction is specifically mediated by the third PDZ domain (PDZ3) of PTPN13 [1], [26], [27]. Since PRK2 is the known physiological ligand of the PDZ3 domain of PTPN13, it is regarded as a class III representative. It is however also interesting to note, the PDZ3 domain of PTPN13 can also bind to class I ligands *in vitro* [1], [28].

Based on the previously published NMR assignments, we now report here the structure in solution of the extended 12.7 kDa PDZ3 domain of PTPN13, which encompasses 119 residues, both in the apo-state and the PRK2-bound form [28]. This PDZ domain shares the highest sequence similarity with the PDZ1 domain of the murine PSD95. As the structural data on class III PDZ domains are rather sparse, the molecular basis of the interaction between the PDZ3 domain of PTPN13 and its physiological ligand PRK2 will further fundamentally contribute to our understanding of PDZ ligand selectivity in general. These data will also provide the basis to analyse a potential functional cross-talk between individual PDZ domains within the scaffolding protein PTPN13 that will help to understand the molecular basis for the selective recognition of ligands by the PDZ3 domain of PTPN13.

Materials and Methods

Protein Expression and Purification

Cloning, expression, and purification of the PDZ3 and PDZ2/PDZ3 tandem domain of murine PTPN13 has been published previously [28], [29]. The point mutant F31A of PDZ3 was generated through site-directed mutagenesis. The purity and integrity of the protein samples were checked by SDS-PAGE. Briefly, the PDZ3 construct used in this study consists in total of 119 amino acids, comprising 16 residues from the PDZ2-PDZ3 linker regions, 89 residues that constitute the canonical PDZ3 domain, and a further 14 residues, of which 9 belong to the linker between PDZ domains 3 and 4; the 5 remaining residues are artefacts from cloning the GST-PDZ3 fusion protein. For complex formation, a tenfold excess of the dodecapeptide MFRDFDYYIADWC derived from the last twelve carboxy-terminal amino acids of the protein kinase c-related protein kinase II (PRK2) was used.

NMR Spectroscopy

Typically, NMR samples contained up to 1 mM of protein in 137 mM NaCl, 2.7 mM KCl, 10 mM Na_2HPO_4, 1.4 mM KH_2PO_4, 0.02 % NaN_3, pH 7.4, and protease inhibitors (complete mini, EDTA-free; Roche). NMR spectra were acquired at 298 K on Bruker DRX 600 and AVANCE III HD 700 spectrometers [30], [31], [32], [33]. Backbone assignments were obtained from three-dimensional HNCA, HN(CO)CA, CBCA(CO)NH, and HNCO spectra [34]. Side-chain assignments were obtained from three-dimensional ^{1}H-^{15}N HNHA [35], [36], ^{1}H-^{13}C HCCH-COSY [37], [38] ^{1}H-^{13}C HCCH-TOCSY [38], ^{1}H-^{13}C NOESY-HSQC [39], ^{1}H-^{15}N NOESY-HSQC, and ^{1}H-^{13}C-NOESY-HSQC [40] spectra. All spectra were processed with nmrPipe [41]

and analysed with nmrView [42] as well as CcpNmr [43]. In addition, heteronuclear $^{15}N\{^{1}H\}$-NOE data were recorded in order to extract pico- to nanosecond dynamics [44] Additionally, ^{1}H-^{13}C HSQC spectra were recorded on a sample containing 15% ^{13}C for the stereospecific assignment of the Val and Leu methyl groups as described previously [45]. Intermolecular NOEs were extracted from filter-edited NOESY spectra and from a ^{1}H-^{13}C-NOESY-HSQC without ^{13}C decoupling in the indirect dimension [46]. The PRK2 resonances in complex with PDZ3 of PTPN13 were assigned based on 2D (transferred) ^{1}H-^{1}H NOESY as well as in a 2D ^{1}H-^{1}H double half filter (DHF) NOESY spectra [47]. Assignments have been published previously and have been deposited in the BioMagResBank (http://www.bmrb.wisc.edu) under accession numbers BMRB-16879 [28].

Structure calculation

Peaks from the NOESY spectra were picked manually, integrated, and partially assigned using nmrView [42]. Then, CYANA was used for automatic NOE assignment and initial structure calculations were based on the unassigned NOESY peak lists and dihedral angle restraints as input data obtained from TALOS [48]; [49]. In detail, an ensemble of 20 structures was calculated from a consensus restraint list obtained from 20 individual automatic NOESY assignments/structure calculation runs. The chemical shift tolerances for NOESY peak assignments were set to 0.03 ppm for ^{1}H and to 0.4 ppm for ^{15}N and ^{13}C. For the individual structure calculations, 100 random starting structures were calculated with 10,000 annealing steps using a torsion angle dynamics protocol. Afterwards, the experimental restraints were used to calculate 400 structures from an extended strand by simulated annealing in XPLOR-NIH [50], [51], [82]. The resulting structures were

further refined for energy minimization and the 50 lowest energy structures without NOE violations greater than 0.5 Å and without dihedral angle violations greater than 5° were selected for final structure refinement in explicit water [52]. After water refinement, a validation using PROCHECK-NMR was carried out and the 20 lowest energy structures were chosen to represent the final structure bundle [53]. The statistics for the final ensembles of structures of PDZ3 from PTPN13 both in its free and PRK2-bound form are listed in Table 1. The final coordinates for both the apo-PDZ3 of PTPN13 and the PRK2/PDZ3 complex have been deposited at the Protein Data Bank (www.rcsb.org) under the PDB-ID accession numbers 6GBD and 6GBE, respectively.

Synthetic Peptide

The carboxy-terminal peptide from PRK2, which comprises the sequence H-MFRDFDYIADWC-OH and includes an acetylated amino-terminus, an acetylated carboxy-terminally modified derivate thereof (H-MFRDFDYIADWV-OH, C0V), as well as the APC-derived acetylated dodecapeptide KRHSGSYLVTSV-OH were purchased from JPT Peptide Technologies GmbH, Germany. Peptide stock solutions of at least 7 mM for titration experiments were prepared by dissolving a defined amount of peptide in 137 mM NaCl, 2.7 mM KCl, 10 mM Na_2HPO_4, 1.4 mM KH_2PO_4, 8 mM DTT, 0.02 % NaN_3, pH 7.4. The titrations were carried out by adding increasing amounts of peptide stock solution to the NMR sample containing typically 0.1 mM of protein and NMR spectra were recorded after thorough mixing of the PDZ3 peptide solution. PDZ3 ligand affinity calculations based on observed NMR chemical shift perturbations were carried out using the Origin software package (OriginLab Corp., MA, USA) [54].

Results

Structure of apo-PDZ3 of murine PTPN13

The NMR spectra of PDZ3 of murine PTPN13 are well dispersed (Figs. 2, 3). In total, 1291 NOE distance restraints, consisting of 783 short-range, 178 medium-range, and 330 long-range NOEs, as well as 184 dihedral angle restraints were used during the Xplor-NIH calculations of the apo-PDZ3 structure. The precision of all structural ensembles of PDZ3 is high as judged by the rmsd values (Table 1). The root mean square deviation (rmsd) of the PDZ3 domain based on 40 backbone atoms primarily located in secondary structure elements (14-20, 29-31, 46-51, 56-72, and 98-104) is 0.36 Å +/- 0.06 Å for the ensemble of 20 structures obtained from Xplor-NIH (Table 1; Fig. 6 a). The PDZ3 heavy atom rmsd based on the same selection of 40 residues as mentioned above is 0.98 Å +/- 0.13 Å for the ensemble obtained using Xplor-NIH (Table 1). Unstructured regions however, such as the GLGF motif and amino acids following the EB-β-sheet in the free PDZ3 domain (but not in the PDZ3/PRK2 complex structure) mostly exhibit dynamics on the pico- to nanosecond time scale according to the analysis of the heteronuclear steady-state $^{15}N\{^{1}H\}$-NOE data and, therefore, do not converge during structure computation (Figs. 5, 6A, 7C). The structure in solution of apo-PDZ3 of murine PTPN13 adopts the canonical PDZ fold (Fig. 6a). The overall rmsd between the solutions structures of PDZ3 and PDZ2 (PDB-Code: 1GM1) domains of PTPN13 is 2.3 Å (Fig. 6b). The classical or canonical topology of PDZ domains is characterised by a compact, globular D/E fold, which contains six E-β strands (EA to EF) and two D-α helices (DA, DB) [4], [5]. All of these structural elements are present in apo-PDZ3 of murine PTPN13 except for the short EE β-strand: (EA: T15-F21; EB: F29-R33; EC: I46-

L52; ED: D68-V73; EF: E96-C102; DA: P57-S61; DB: Q83-R91) (Fig. 6a). Like all PDZ domains, the carboxy- and amino-terminal residues of PDZ3 are located in close proximity on the opposite site of the ligand binding cleft. PDZ domains are small protein modules that consist of approximately 90 amino acids and they are known to bind linear carboxy-terminal motifs of their corresponding physiological ligand with high selectivity [6], [13], [55]. Using NMR spectroscopy, we found a bivalent binding selectivity for the PDZ3 domain of PTPN13. Not only does it recognise PRK2, a class III ligand, but also APC, a member of the ligand class I known to interact with PDZ2 of PTPN13 [1]. Based on NMR chemical shift perturbation titrations experiments using ^{15}N-enriched PDZ3 of PTPN13, we determined K_D values of 318 ± 47 µM for a PRK2-derived dodecapeptide and 721 ± 148 µM for a APC-derived dodecapeptide KRHSGSYLVTSV, a tumor suppressor that regulates the actin cytoskeleton and is involved in cell adhesion [56] (Figs. 2, 3). In the PDZ2/PDZ3 tandem domain however, the affinity of PDZ3 for the APC-derived dodecapeptide dropped to approximately 1 mM. The structure of PDZ3 from PTPN13, both in its free and peptide-complex form, now further expands the molecular basis of how class III PDZ domains, select, interact, and recognise their physiological class II ligands, such as PRK2, at atomic resolution.

Structure in solution of the PDZ3 domain of murine PTPN13 in complex with the carboxy-terminal peptide derived from PRK2

The rmsd of the PDZ3/PRK2 complex based also on 40 backbone atoms (15-20, 29-32, 46-52, 63-77, and 96-103) is 0.51 Å +/- 0.09 Å for structures computed using Xplor-NIH (Table 1; Fig. 7). Based on the heavy atoms of those selected atoms of the PDZ3/PRK2 complex, the rmsd of the complex is 1.16 Å +/- 0.17 Å for the

ensemble generated by Xplor-NIH (Table 1; Fig. 7). The slightly lower precision of the PDZ3/PRK2 complex structure in comparison to the structure of apo-PDZ3 can be attributed to the micromolar affinity of PDZ3 for PRK2 as this required a molar excess of the PRK2 peptide to PDZ3 of 1:10. For the calculation of the PDZ3/PRK2 complex, 1170 NOE distance restraints, comprising 779 short-range, 129 medium-range, 246 long-range, and 14 intermolecular NOEs, as well as 178 dihedral angle restraints could be extracted from NOESY spectra. The 14 intermolecular NOEs (Fig. 7 A, B) could be detected between residues G26, S30-S32, Q83, I87, and L90 of PDZ3 and C0, W-1, D-2, I-4 of PRK2 (Fig. 7 A, B). These intermolecular NOEs clearly define the interaction site as well as the binding mode of the PRK2-derived peptide and the PDZ3 domain from PTPN13 (Fig. 7 B). In comparison to the calculation of apo PDZ3, the number of long-range NOEs declined from 330 to 246. Nonetheless, the overall precision of structures is still high and allows for the analysis of the molecular basis of PRK2 recognition by PDZ3 of PTPN13. Like its apo form, the compact globular α/β fold PDZ3 of murine PTPN13 in complex with PRK2 consists of five β-strands and two α-helices (Fig. 7). In contrast to the apo-PDZ3 structure, GLGF motif and most of the amino acids following the EB-β-sheet in the PDZ3/PRK2 complex structure are rigidified as they do not exhibit dynamics on the pico- to nanosecond time scale according to the analysis of the heteronuclear steady-state $^{15}N\{^{1}H\}$-NOE data (Fig. 5).

Structural basis of the recognition of the PRK2 carboxy-terminus by PDZ3

The structure of the PDZ3/PRK2 complex presented here reveals the molecular basis of the interaction between the carboxy-terminal peptide of PRK2 and the PDZ3 domain of PTPN13 at atomic resolution (Fig. 7 B, C). Complex formation is

mainly mediated through the highly conserved GLGF motif found in these PDZ proteins, which stabilizes the carboxylic function, denoted as P0, of the PDZ-ligand carboxy-terminus itself. This interaction is accomplished by three hydrogen bonds between carboxylic oxygen atoms from the peptide ligand and LGF amide groups located within the PDZ protein's GLGF motif. In some PDZ domains additional interactions with their ligands have been described, facilitated by a conserved K or R side chain positioned four amino acids in front of the GLGF motif towards the amino-terminus (K/RXXXGLGF) [4]. In PDZ/peptide complexes, the last four carboxy-terminal amino acids from the ligand bind to a cleft of the PDZ domain located between the EB-β sheet and the DB-α helix and thereby extend the antiparallel E-β sheet [4], [57]. While the amino acid side chains in position P-1 and P-3 of the ligand point away from the PDZ binding cleft, the amino acid side chains of P0 und P-2 are oriented towards the PDZ binding pocket. Therefore, positions P0 und P-2 influence and/or control the ligand's selectivity for PDZ domain(s) to a greater extend [58]. According to NMR titration experiments, the K_D value for the PDZ3/PRK2 complex is at the lower end of affinities reported for PDZ/peptide interactions ([59]) (Fig. 3). Further, we also show here that this PDZ3 domain also binds to the carboxy-terminus of APC, albeit with an extremely low affinity (Fig. 2). The structure of the PDZ3/PRK2 complex now reveals some particular features that explain this lower affinity and the observed promiscuity of PDZ3 of PTPN13, but it can now also explain as to why PDZ3 selects PRK2 over APC as a ligand. Firstly, the GLGF loop of class III PDZ domains is less conserved. Secondly, numerous PDZ domains are characterized by an extension of the classical GLGF motif to K/RXXXGLGF that further stabilizes the interactions with their ligands through coordinating a water molecule. A characteristic NOE network supporting this

extended interaction between the PDZ3 domain of PTPN13 and PRK2 however, could not be identified. In the NMR ensemble of the PDZ3/PRK2 complex, the side chain of the conserved K22 of PDZ3 does not point towards the PRK2 ligand. Instead, the side chain of K22 is partly rotated out of the binding site upon interacting with PRK2 to provide more space in the binding cleft of PDZ3 of PTPN13 (Fig. 8). An analysis of all class III PDZ3 domains published to date suggests that the stabilization of the bound ligand through the amino acid side chain of a conserved K or R located in the extended K/RXXXGLGF motif only plays a minor role. Structures of PDZ domains from nNos (PDB-Code: 1B8Q) and Afadin (PDB-Code: 2AIN) show similar side chain conformations of K or R like K22 in PDZ3 of PTPN13. The same holds true even for the apo-PDZ structures of RIL (PDB-Code: 2EEG) and, in part, Mint1 (PDB-Code: 1U37), whose conserved K or R side chains also do not point towards the peptide ligand binding site. Interestingly, this amino acid position is not even conserved in the PDZ domains of Zasp (PDB-Code: 1RGW) and Syntenin1 (PDB-Code: 1W9O). Another notable feature of the PDZ3 domain of PTPN13 is F31, positioned two amino acids carboxy-terminal after the GLGF motif (GLGFSF) (Fig. 1). In contrast to the other sequences from all PDZ domain classes aligned in Fig. 1, PDZ3 of PTPN13 contains an aromatic side chain at this position, whereas an aliphatic residue is usually found a this position of the EB-β-sheet (Fig. 1, 9). This results in a rather shallow binding cleft between the EB-β-sheet and the DB-α helix of the PDZ3 domain from PTPN13 in comparison to other PDZ domains (Fig. 9). The aromatic ring system of F31 lies within the plane of the EB β-strand and, together with V86 and I87, flattens the ligand binding cleft of PDZ3 of PTPN13 to further reduce its binding interface area (Fig. 9). A F31A mutant of PDZ3 destabilizes the PDZ fold

and/or lead to aggregation of PDZ3 and a dramatically reduced ligand affinity as judged from ^{1}H-^{15}N HSQC NMR spectra (Fig. 4). The interaction between PDZ domains and their ligands is in particular mediated by a hydrogen bond between the amino acid side chain at position P-2 of the peptide ligand and a side chain NH of a conserved histidine residue located at the beginning of DB α-helix in the PDZ protein as numerous studies have shown [18], [20]. Noteworthy, this histidine residue is not present in PDZ3 of PTPN13 (Fig. 1). Instead, this PDZ domain contains a glutamine residue (Q83) at this position, which is capable of stabilizing the side chain carboxylate function of the ligand in position P-2 of PRK2 through a hydrogen bond (Figs. 1, 8-10). Although the PRK2/PDZ3 interaction principally differs at this position from the classical PDZ-ligand binding mode, it is yet functionally conserved. The orientation of the PRK2 peptide in the binding pocket of PDZ equals the canonical binding mode (Figs. 1, 8-10). The free carboxy-terminus of the ligand cysteine residue located at position P0 (C0) is stabilised by hydrogen bonds to the backbone amide groups of L27 and G28, whereas the carbonyl group of F29 forms a hydrogen bond with the amide group of C0 (Figs. 3, 8-10). The ligand side chains of cysteine and aspartate at positions P0 and P2 are oriented towards the PDZ binding cleft, whereas those in P-1 and P-3, tryptophan and alanine are facing towards the solvent (Figs. 1, 8-10). A mutant PRK2 peptide with valine instead of cysteine in P0 (C0V) binds to PDZ3 with 38% higher affinity (Fig. S2). Apparently, PDZ3 of murine PTPN13 not only tolerates ligands carrying a carboxy-terminal cysteine but also valine. The cysteine of PRK2 contacts N23 and G26 in PDZ3. The bulky tryptophan side chain in P-1 can probably not be accommodated by the PDZ3 ligand binding site that contains three large side chains, F31, V86, and I87. The solvent exposed P-1 tryptophan rather packs

against L27 of PDZ3 and the alanine side chain in position -3 of the PRK2 ligand. The aspartate side chain in position P-2 of the PRK2 ligand is buttressed by a hydrogen bond originating from the Q83 side chain of the DB α-helix (Figs. 1, 8-10). In the nNos structure (PDB-Code: 1B8Q), the P-2 aspartate side chain is stabilised by a tyrosine hydroxyl group. In the ZO1 PDZ3 in complex with a phage-derived class peptide (PDB-Code: 4Q2Q), the P-2 aspartate side chains points away from the PDZ binding cleft leading to non-canonical bent and therefore not extended β-sheet ligand conformation [17]. Taken together, the interaction between PDZ3 and the PRK2 carboxy-terminus comprises five PRK2 residues and extends until position P-4 as its Ile side chain is in proximity to the side chains of E34 and I87 in PDZ3. In comparison to most canonical PDZ class I, II, and even the few known class III interactions, the PDZ3/PRK2 binding interface is thus lengthened by one ligand residue [60].

Discussion

Like PTP, PH, SH2, and SH3 domains, PDZ domains are important cellular mediators of protein-protein interactions. PDZ domain-containing proteins play important roles in complexing and anchoring transmembrane proteins as well as in morphogenesis [13]; [15]; [61]. The human protein tyrosine phosphatase PTPN13 is also involved in numerous cellular processes, such as regulation of cytokinesis and signal transduction [62]; [63]; [64]; [65]; [66]. PTPN13 harbours five consecutive PDZ domains, termed PDZ1 to PDZ5. Based on yeast two-hybrid assays and co-immunoprecipitation experiments from transfected HeLa cells, PDZ3 of PTPN13 has been described to interact with protein kinase PRK2, a regulator of the cell cycle [1], [27].

Several approaches have been described to classify PDZ domains and their ligands [18], [19], [20], [23], [25], [57], [67], [68], [69]. However, the analysis focused on PDZ domains that significantly differ from PDZ3 of PTPN13 in almost all cases. Therefore, our structural studies shed light on the mechanism of how PDZ3 selects and bind its physiological ligand at atomic resolution. According to Stiffler and Chen, PDZ3 of PTPN13 qualifies as a class III PDZ domain [67] and 16 crucial amino acids constitute the peptide binding cleft: G26, L27, G28, F29, S30, F31, S32, R33, K50, K51, F53, Q83, Q84, I87, and T93. This peptide binding pocket is corroborated by 14 intermolecular NOEs that include G26, S30-S32, Q83, I87, and L90 of PDZ3 and C0, W-1, D-2, I-4 of PRK2 (Fig. 7 B). Based on NMR chemical shift perturbation experiments, we could show that the affinity of PDZ3 from PTPN13 is 318 ± 47 µM for a PRK2-derived dodecapeptide and 721 ± 148 µM for a APC-derived dodecapeptide KRHSGSYLVTSV, a tumor suppressor that regulates the actin cytoskeleton and is involved in cell adhesion [56]. The biggest difference

between the PDZ2 and PDZ3 binding clefts from PTB-BL is indeed F31 in PDZ3, which is a valine in PDZ2 and thus renders its binding pocket more open (Fig. 9). More importantly, Q83 in PDZ3 is changed to His78 in PDZ2. These two changes might account for PDZ3 selecting PRK2 over APC as the interaction between Q83 and P-2 of the ligand peptide is presumably optimised in PDZ3 for PRK2 that bears D in P-2 instead of T as found in APC (Fig. 10). In spite of the low affinity, APC could still be of regulatory and therefore physiological significance for PDZ3 of PTPN13 as an increasing number of identified weak protein complexes emerge as essential components in physiological processes [70]. According to Stiffler and Chen, I-4, A-3, D-2, W-1, and C0 have been identified as important residues in PRK2 – a class III ligand – that is recognized by PDZ from PTPN13. For the class I ligand APC, residues L-4, V-3, T-2, S-1, and V0 are predicted to be important for interaction with PDZ3 from PRP-BL [67].

According to Kalyoncu and coworkers, PDZ domains can be classified according to three conserved amino acid sequence elements [69]. The first element is located in the PDZ-peptide binding interface that comprises the GLGF loop [61] and the second one is found at the end of the DB-α-helix [71]. Surprisingly, the highly conserved histidine – or any other hydrogen bond donor for the P-2 ligand amino acid – positioned at the beginning of the DB-α-helix does not play a significant role in this analysis. This is presumably due to the fact that the two neighbouring positions of this histidine residue are much less conserved. The third conserved element, which is located in front of the ED-β-sheet [72], is not part of the peptide binding interface of PDZ domains either. The importance of this element for ligand selection is still not fully understood but it has been suggested to participate in the dimerisation of PDZ domains [72]. It is interesting to note, that

PDZ3 of PTPN13 does contain all of these three conserved elements although it is a class III member, a class not covered by the analysis reported by Kalyoncu [69]. In PDZ3 of PTPN13, these three elements correspond to the following residues: G28/F29 of the GLGF loop, L90/R91 of the DB-α-helix, and G67/D68 preceding the ED-β-sheet. In spite of an identical topology, subtle structural differences can be even found for the carboxylate-binding loop and the DB-α helix of the PDZ ligand pocket. Together with the differences in the amino acid sequence of the carboxylate-binding loop, this structural divergence could contribute to the selection of PRK2 over APC by PDZ3 from PTPN13. The rmsd for the backbone atoms of 40 amino acids mainly located in secondary structure elements of the structure ensemble of PDZ3 is 0.43 Å +/- 0.12 Å and the rmsd of the heavy atoms of the these 40 amino acids is 0.90 Å +/- 0.14 Å. In the structure ensemble of the PDZ3/PRK2-complex, the rmsd for the backbone atoms of 40 amino acids mostly located in secondary structure elements is 0.51 Å +/- 0.17 Å and the rmsd of the heavy atoms of the these 40 amino acids is 1.16 Å +/- 0.17 Å (Fig. 7). Noteworthy, the W-1 of the PRK2 peptide bound to PDZ from PTPN13 is solvent exposed. The aromatic ring system of F31 lies within the plane of the EB β-strand and flattens the ligand binding cleft of PDZ3 of PTPN13 to further reduce its binding interface area (Fig. 9). Presumably, this contributes to the rather low micromolar binding affinity of PDZ to class III ligands in comparison to other PDZ domains. The mutation experiments clearly show on the one hand that the PRK2 C0V mutant peptide binds to PDZ3 with a slightly higher affinity. On the other hand, the F31A mutant of PDZ3 destabilizes the PDZ fold and/or leads to aggregation of PDZ3 and a dramatically reduced ligand affinity with a K_D value well above 1 mM (Fig. 4 A, B). The former shows that the PDZ3 binding cleft is capable of accommodating the isopropyl side

chain of valine, which – in contrast to the wildtype PRK2 cysteine –apparently contributes to increased van der Waals contacts within the PDZ3 binding pocket that strengthen the PDZ3/PRK2 interaction. This is in accordance with a previous phage display study that found a preference of PDZ3 for valine in position 0 [84]. The latter suggests that F31 not only changes and flattens the PDZ binding cleft to determine binding specificity but is also an important core residue of PDZ3 that stabilises both the binding pocket and even the entire PDZ3 fold. Taken together, the mutation data indeed underline the crucial role of both F31 from PDZ3 and C0 from PRK2 in determining the binding affinity of the PDZ3/PRK2 complex. Nonetheless, the interaction between PDZ3 and the PRK2 carboxy-terminus ranges from the carboxy-terminal cysteine in P0 to isoleucine in position P-4, which is surrounded by E34 and I87 from PDZ3. In comparison to class I and II ligand recognition, this class III PDZ3/PRK2 interface is extended, which concurs with previous observations [57], [60], [67], [73]. Upon binding, the carboxy-terminus of PDZ domain ligand adopt an E-β strand conformation that extends the existing anti-parallel, two-stranded E-sheet found in the apo-PDZ domain – a mechanism referred to as E-strand addition [74]. However a complete NOE pattern indicative of an E-strand could not be extracted from the NOESY spectra of the PDZ3/PRK2 complex. Nonetheless the PRK2 peptide also adopts an extended conformation upon binding to PDZ3 (Fig. 7). Interestingly, the structural differences between the free and PRK2-bound PDZ3 domain from PTPN13 are not located in and near the peptide-binding cleft but further extent to remote regions in this PDZ domain (Figs. 8, 9). In addition, the titration of the APC peptide with the PDZ2/3 tandem domain yields a K_D value of approximately 1 mM and thus an even weaker interaction in comparison to the single PDZ3 domain (Fig. S1 a, b). Apparently, not only binds

APC to PDZ2 but this also weakens the interaction between PDZ3 and APC despite the linker of 44 residues between both PDZ domains in PTPN13. This could suggest allosteric effects mediated by PDZ2/PDZ3 domain interactions to potentially modulate ligand recognition of and binding to PTPN13, a feature not unprecedented in PDZ-ligand interactions [75], [76], [77], [78], [79], [80], [85]. For PTPN13, however, future experiments are required to prove this hypothesis further.

In summary, the structure in solution of PDZ3 from murine PTPN13 and in complex with a PRK2-derived carboxy-terminal peptide expand the currently rather limited knowledge about the interaction between a class III PDZ domain and a class III peptide ligand. The structures presented here shed light on a molecular level as to why PDZ3 of PTPN13 exhibits a rather weak affinity for its class I and III ligands, APC and PRK2. Recently, a study on the binding promiscuity of the PDZ domain from the neuronal NO Synthase reported that it even binds to ligands of all three classes [60]. Lastly, the apo- and complex structures of PDZ3 from PTPN13 now provide the molecular basis for further studies on its rather low level of ligand selectivity and on its low-affinity for new (peptide) ligands. Finally, our study complements the wealth of structural information previously published for the PDZ2 domain of PTPN13 [81]; [3]. In total, PTPN13 contains five PDZ domains that are separated by linkers of different length and it has been suggested that PTPN13 acts as a scaffolding protein in the cell, because each PDZ domain can interact with different ligands [1]. Future studies will have to address the important question as to whether the relative PDZ1-5 domain orientations differ from one another upon

binding to various ligands. Evidently, this will have profound functional, PDZ domain-mediated physiological implications for PTPN13.

Conclusion

PDZ domains are common protein-protein-interaction-domains sharing a globular fold. They preferentially bind the carboxy-termini of their ligand proteins with high specificity. Since PDZ domain proteins often consist of more than one PDZ domain they are referred to as scaffolding proteins, harbouring large macromolecular protein complexes. These complexes are involved in numerous regulatory cellular processes. PDZ3 of PTPN13 belongs to the unusual class III PDZ domains, which bind to ligands harbouring the carboxy-terminal motif -X-D/E-X-Φ-COOH. The structures PDZ3 of murine PTPN13 bound to the carboxy-terminus of PRK2 now represent a rare example of selective class III ligand recognition by a PDZ domain now provide a basis for the detailed structural investigation of the promiscuous interaction between the PDZ domains of PTPN13 and of their interaction with ligands. PDZ3 of PTPN13 adopts the common D/E-fold without the short EE-strand. PDZ3 of PTPN13 binds five carboxy-terminal amino acids of PRK2 *via* a groove located between the EB-strand and the DB-helix to achieve selectivity. The PRK2 peptide binds to the canonical PDZ3 binding cleft in an elongated manner and its amino acid side chains in position P0 and P-2, cysteine and aspartate, face the groove between EB-strand and DB-helix of PDZ3, whereas the PRK2 side chains of tryptophan and alanine located in position P-1 and P-3 point away from the binding pocket. These PDZ3 structures now provide a molecular basis for the design of biochemical experiments and molecular dynamics studies in the future that will ultimately help to decipher PTPN13's scaffolding function(s) and selectivity determinants of PDZ domains for (novel) class III ligands in general. In addition, the structures of PDZ3, both in its free and PRK2-complexed form, might ultimately contribute to the development of low molecular weight antagonists that could even

act on the protein kinase C-related kinase-2 (PRK2) signalling pathway to modulate rearrangements of the actin cytoskeleton.

Acknowledgements

We are extremely grateful to Gregor Barchan, Martin Gartmann, and Hans-Jochen Hauswald for expert technical assistance. This work was supported by a DFG grant (ER291/2-1) to R.S and K.S.E. Part of the work was financially supported by the European Commission in the framework of the project INTCHEM (MEST-CT-2005-020681). G. K. has been a fellow of the RUB Research School and M. D. has been supported by a fellowship from the Hans-Böckler-Stiftung. R. S. gratefully recognizes generous support from the DFG (213/757-1 FUGG), BMBF, Fonds der Chemischen Industrie (FCI), Proteincenter (NRW center of excellence), RUB Protein Research Department, RUB Interfacial Systems Chemistry Research Department, and RUBiospek.

References

[1] Erdmann KS. The protein tyrosine phosphatase PTP-Basophil/Basophil-like. Interacting proteins and molecular functions. Eur J Biochem. 2003;270:4789-98.

[2] Kachel N, Erdmann KS, Kremer W, Wolff P, Gronwald W, Heumann R, et al. Structure determination and ligand interactions of the PDZ2b domain of PTP-Bas (hPTP1E): splicing-induced modulation of ligand specificity. Journal of molecular biology. 2003;334:143-55.

[3] Walma T, Aelen J, Nabuurs SB, Oostendorp M, Van Den Berk L, Hendriks W, et al. A closed binding pocket and global destabilization modify the binding properties of an alternatively spliced form of the second PDZ domain of PTP-BL. Structure. 2004;12:11-20.

[4] Doyle DA, Lee A, Lewis J, Kim E, Sheng M, MacKinnon R. Crystal structures of a complexed and peptide-free membrane protein-binding domain: molecular basis of peptide recognition by PDZ. Cell. 1996;85:1067-76.

[5] Cabral JoHM, Petosa C, Sutcliffe MJ, Raza S, Byron O, Poy F, et al. Crystal structure of a PDZ domain. 1996.

[6] Sheng M, Sala C. PDZ domains and the organization of supramolecular complexes. Annual review of neuroscience. 2001;24:1-29.

[7] Maekawa K, Imagawa N, Naito A, Harada S, Yoshie O, Takagi S. Association of protein-tyrosine phosphatase PTP-BAS with the transcription-factor-inhibitory protein IkappaBalpha through interaction between the PDZ1 domain and ankyrin repeats. Biochem J. 1999;337 (Pt 2):179-84.

[8] Nakai Y, Irie S, Sato TA. Identification of IkappaBalpha as a substrate of Fas-associated phosphatase-1. Eur J Biochem. 2000;267:7170-5.

[9] Irie S, Hachiya T, Rabizadeh S, Maruyama W, Mukai J, Li Y, et al. Functional interaction of Fas-associated phosphatase-1 (FAP-1) with p75(NTR) and their effect on NF-kappaB activation. FEBS Lett. 1999;460:191-8.

[10] Zimmermann P, Meerschaert K, Reekmans G, Leenaerts I, Small JV, Vandekerckhove Jl, et al. PIP 2-PDZ domain binding controls the association of syntenin with the plasma membrane. Molecular cell. 2002;9:1215-25.

[11] Oliva C, Escobedo P, Astorga C, Molina C, Sierralta J. Role of the MAGUK protein family in synapse formation and function. Dev Neurobiol. 2012;72:57-72.

[12] González-Mariscal L, Betanzos A, Avila-Flores A. MAGUK proteins: structure and role in the tight junction. Semin Cell Dev Biol. 2000;11:315-24.

[13] Kornau H-C, Schenker LT, Kennedy MB, Seeburg PH. Domain interaction between NMDA receptor subunits and the postsynaptic density protein PSD-95. Science. 1995;269:1737.

[14] Cho K-O, Hunt CA, Kennedy MB. The rat brain postsynaptic density fraction contains a homolog of the Drosophila discs-large tumor suppressor protein. Neuron. 1992;9:929-42.

[15] Woods DF, Bryant PJ. ZO-1, DlgA and PSD-95/SAP90: homologous proteins in tight, septate and synaptic cell junctions. Mechanisms of development. 1993;44:85-9.

[16] Itoh M, Nagafuchi A, Yonemura S, Kitani-Yasuda T, Tsukita S. The 220-kD protein colocalizing with cadherins in non-epithelial cells is identical to ZO-1, a tight junction-associated protein in epithelial cells: cDNA cloning and immunoelectron microscopy. The Journal of Cell Biology. 1993;121:491-502.

[17] Ernst A, Appleton BA, Ivarsson Y, Zhang Y, Gfeller D, Wiesmann C, et al. A structural portrait of the PDZ domain family. J Mol Biol. 2014;426:3509-19.

[18] Vaccaro P, Dente L. PDZ domains: troubles in classification. FEBS Lett. 2002;512:345-9.

[19] Nourry C, Grant SG, Borg JP. PDZ domain proteins: plug and play! Sci STKE. 2003;2003:RE7.

[20] Bezprozvanny I, Maximov A. Classification of PDZ domains. Febs Letters. 2001;509:457-62.

[21] Jaffrey SR, Snowman AM, Eliasson MJL, Cohen NA, Snyder SH. CAPON: a protein associated with neuronal nitric oxide synthase that regulates its interactions with PSD95. Neuron. 1998;20:115-24.

[22] Zheng M, Cheng H, Banerjee I, Chen J. ALP/Enigma PDZ-LIM domain proteins in the heart. Journal of molecular cell biology. 2009:mjp038.

[23] Radziwill G, Weiss A, Heinrich J, Baumgartner M, Boisguerin P, Owada K, et al. Regulation of c-Src by binding to the PDZ domain of AF-6. EMBO J. 2007;26:2633-44.

[24] Jeleń F, Oleksy A, Śmietana K, Otlewski J. PDZ domains-common players in the cell signaling. Acta Biochimica Polonica. 2003;50:985-1017.

[25] Giallourakis C, Cao Z, Green T, Wachtel H, Xie X, Lopez-Illasaca M, et al. A molecular-properties-based approach to understanding PDZ domain proteins and PDZ ligands. Genome Res. 2006;16:1056-72.

[26] Vincent S, Settleman J. The PRK2 kinase is a potential effector target of both Rho and Rac GTPases and regulates actin cytoskeletal organization. Mol Cell Biol. 1997;17:2247-56.

[27] Gross C, Heumann R, Erdmann KS. The protein kinase C-related kinase PRK2 interacts with the protein tyrosine phosphatase PTP-BL via a novel PDZ domain binding motif. FEBS letters. 2001;496:101-4.

[28] Kock G, Dicks M, Heumann R, Erdmann KS, Stoll R. Sequence-specific 1H, 13C, and 15N assignment of the extended PDZ3 domain of the protein tyrosine phosphatase basophil-like PTP-BL. Biomol NMR Assign. 2010;4:199-202.

[29] Fetzer CP, Sauvageau J, Kock G, Berghaus C, Bangert JA, Dicks M, et al. Sequence-specific (1)H, (13)C, and (15)N backbone assignment of the 28 kDa PDZ2/PDZ3 tandem domain of the protein tyrosine phosphatase PTP-BL. Biomol NMR Assign. 2007;1:151-3.

[30] Stoll R, Renner C, Ambrosius D, Golob M, Voelter W, Buettner R, et al. Sequence-specific 1H, 13C, and 15N assignment of the human melanoma inhibitory activity (MIA) protein. J Biomol NMR. 2000;17:87-8.

[31] Nowaczyk M, Berghaus C, Stoll R, Roegner M. Preliminary structural characterisation of the 33 kDa protein (PsbO) in solution studied by site-directed mutagenesis and NMR spectroscopy. Physical Chemistry Chemical Physics. 2004;6:4878-81.

[32] Stoll R, Lee BM, Debler EW, Laity JH, Wilson IA, Dyson HJ, et al. Structure of the Wilms tumor suppressor protein zinc finger domain bound to DNA. J Mol Biol. 2007;372:1227-45.

[33] Rehmann H, Bruning M, Berghaus C, Schwarten M, Kohler K, Stocker H, et al. Biochemical characterisation of TCTP questions its function as a guanine nucleotide exchange factor for Rheb. FEBS Lett. 2008;582:3005-10.

[34] Grzesiek S, Bax A. Correlating backbone amide and side chain resonances in larger proteins by multiple relayed triple resonance NMR. Journal of the American Chemical Society. 1992;114:6291-3.

[35] Vuister GW, Bax A. Quantitative J correlation: a new approach for measuring homonuclear three-bond J(HNH.alpha.) coupling constants in 15N-enriched proteins. Journal of the American Chemical Society. 1993;115:7772-7.

[36] Vuister GW, Bax A. Measurement of four-bond HN-H alpha J-couplings in staphylococcal nuclease. J Biomol NMR. 1994;4:193-200.

[37] Kay LE, Ikura M, Bax A. Proton-proton correlation via carbon-carbon couplings: a three-dimensional NMR approach for the assignment of aliphatic resonances in proteins labeled with carbon-13. Journal of the American Chemical Society. 1990;112:888-9.

[38] Kay LE, Xu GY, Singer AU, Muhandiram DR, Formankay JD. A gradient-enhanced HCCH-TOCSY experiment for recording side-chain 1 H and 13 C correlations in H 2 O samples of proteins. Journal of Magnetic Resonance, Series B. 1993;101:333-7.

[39] Palmer AG, Cavanagh J, Wright PE, Rance M. Sensitivity improvement in proton-detected two-dimensional heteronuclear correlation NMR spectroscopy. Journal of Magnetic Resonance (1969). 1991;93:151-70.

[40] Davis AL, Keeler J, Laue ED, Moskau D. Experiments for recording pure-absorption heteronuclear correlation spectra using pulsed field gradients. Journal of Magnetic Resonance (1969). 1992;98:207-16.

[41] Delaglio F, Grzesiek S, Vuister GW, Zhu G, Pfeifer J, Bax A. NMRPipe: a multidimensional spectral processing system based on UNIX pipes. J Biomol NMR. 1995;6:277-93.

[42] Johnson BA, Blevins RA. NMR View: A computer program for the visualization and analysis of NMR data. Journal of biomolecular NMR. 1994;4:603-14.

[43] Skinner SP, Goult BT, Fogh RH, Boucher W, Stevens TJ, Laue ED, et al. Structure calculation, refinement and validation using CcpNmr Analysis. Acta Crystallogr D Biol Crystallogr. 2015;71:154-61.

[44] Kay LE, Torchia DA, Bax A. Backbone dynamics of proteins as studied by 15N inverse detected heteronuclear NMR spectroscopy: application to staphylococcal nuclease. Biochemistry. 1989;28:8972-9.

[45] Neri D, Szyperski T, Otting G, Senn H, Wuethrich K. Stereospecific nuclear magnetic resonance assignments of the methyl groups of valine and leucine in the DNA-binding domain of the 434 repressor by biosynthetically directed fractional carbon-13 labeling. Biochemistry. 1989;28:7510-6.

[46] Zwahlen C, Legault P, Vincent SJ, Greenblatt J, Konrat R, Kay LE. Methods for measurement of intermolecular NOEs by multinuclear NMR spectroscopy: application to a bacteriophage λ N-peptide/boxB RNA complex. Journal of the American Chemical Society. 1997;119:6711-21.

[47] Otting G, Wüthrich K. Extended heteronuclear editing of 2D 1 H NMR spectra of isotope-labeled proteins, using the X (ω 1, ω 2) double half filter. Journal of Magnetic Resonance (1969). 1989;85:586-94.

[48] Güntert P, Buchner L. Combined automated NOE assignment and structure calculation with CYANA. Journal of biomolecular NMR. 2015;62:453-71.

[49] Shen Y, Delaglio F, Cornilescu G, Bax A. TALOS+: a hybrid method for predicting protein backbone torsion angles from NMR chemical shifts. Journal of biomolecular NMR. 2009;44:213-23.

[50] Schwieters CD, Kuszewski JJ, Tjandra N, Clore GM. The Xplor-NIH NMR molecular structure determination package. Journal of magnetic resonance. 2003;160:65-73.

[51] Schwieters CD, Kuszewski JJ, Clore GM. Using Xplorâ€“NIH for NMR molecular structure determination. Progress in Nuclear Magnetic Resonance Spectroscopy. 2006;48:47-62.

[52] Linge JP, Williams MA, Spronk CAEM, Bonvin AMJJ, Nilges M. Refinement of protein structures in explicit solvent. Proteins: Structure, Function, and Bioinformatics. 2003;50:496-506.

[53] Laskowski RA, Rullmann JAC, MacArthur MW, Kaptein R, Thornton JM. AQUA and PROCHECK-NMR: programs for checking the quality of protein structures solved by NMR. Journal of biomolecular NMR. 1996;8:477-86.

[54] Fielding L. NMR methods for the determination of protein-ligand dissociation constants. Curr Top Med Chem. 2003;3:39-53.

[55] Hillier BJ, Christopherson KS, Prehoda KE, Bredt DS, Lim WA. Unexpected modes of PDZ domain scaffolding revealed by structure of nNOS-syntrophin complex. Science. 1999;284:812-5.

[56] Erdmann KS, Kuhlmann Jr, Lessmann V, Herrmann L, Eulenburg V, Muller O, et al. The Adenomatous Polyposis Coli-protein (APC) interacts with the protein tyrosine phosphatase PTP-BL via an alternatively spliced PDZ domain. Oncogene. 2000;19:3894-901.

[57] Tonikian R, Zhang Y, Sazinsky SL, Currell B, Yeh J-H, Reva B, et al. A specificity map for the PDZ domain family. PLoS Biol. 2008;6:e239.

[58] Daniels DL, Cohen AR, Anderson JM, Bruenger AT. Crystal structure of the hCASK PDZ domain reveals the structural basis of class II PDZ domain target recognition. Nature Structural & Molecular Biology. 1998;5:317-25.

[59] Jemth P, Gianni S. PDZ domains: folding and binding. Biochemistry. 2007;46:8701-8.

[60] Merino-Gracia J, Costas-Insua C, Canales MÃn, RodrÃguez-Crespo I. Insights into the C-terminal Peptide Binding Specificity of the PDZ Domain of Neuronal Nitric-oxide Synthase CHARACTERIZATION OF THE INTERACTION WITH THE TIGHT JUNCTION PROTEIN CLAUDIN-3. Journal of Biological Chemistry. 2016;291:11581-95.

[61] Roh MH, Margolis B. Composition and function of PDZ protein complexes during cell polarization. American Journal of Physiology-Renal Physiology. 2003;285:F377-F87.

[62] Wansink DG, Peters W, Schaafsma I, Sutmuller RPM, Oerlemans F, Adema GJ, et al. Mild impairment of motor nerve repair in mice lacking PTP-BL tyrosine phosphatase activity. Physiological genomics. 2004;19:50-60.

[63] Prokopenko SN, Saint R, Bellen HJ. Untying the Gordian Knot of Cytokinesis Role of Small G Proteins and Their Regulators. The Journal of cell biology. 2000;148:843-8.

[64] Skop AR, Bergmann D, Mohler WA, White JG. Completion of cytokinesis in C. elegans requires a brefeldin A-sensitive membrane accumulation at the cleavage furrow apex. Current Biology. 2001;11:735-46.

[65] Grunwald IC, Korte M, Wolfer D, Wilkinson GA, Unsicker K, Lipp H-P, et al. Kinase-independent requirement of EphB2 receptors in hippocampal synaptic plasticity. Neuron. 2001;32:1027-40.

[66] Wilkinson DG. Multiple roles of EPH receptors and ephrins in neural development. Nature Reviews Neuroscience. 2001;2:155-64.

[67] Stiffler MA, Chen JR, Grantcharova VP, Lei Y, Fuchs D, Allen JE, et al. PDZ domain binding selectivity is optimized across the mouse proteome. Science. 2007;317:364-9.

[68] Chen JR, Chang BH, Allen JE, Stiffler MA, MacBeath G. Predicting PDZ domainâ€“peptide interactions from primary sequences. Nature biotechnology. 2008;26:1041-5.

[69] Kalyoncu S, Keskin O, Gursoy A. Interaction prediction and classification of PDZ domains. BMC Bioinformatics. 2010;11:357.

[70] Qin J, Gronenborn AM. Weak protein complexes: challenging to study but essential for life. FEBS J. 2014;281:1948-9.

[71] Sudol M. From Src Homology domains to other signaling modules: proposal of theprotein recognition code'. Oncogene. 1998;17:1469-74.

[72] Gianni S, Engstroem Ak, Larsson Mr, Calosci N, Malatesta F, Eklund L, et al. The kinetics of PDZ domain-ligand interactions and implications for the binding mechanism. Journal of Biological Chemistry. 2005;280:34805-12.

[73] Erlendsson S, Rathje M, Heidarsson PO, Poulsen FM, Madsen KL, Teilum K, et al. Protein interacting with C-kinase 1 (PICK1) binding promiscuity relies on unconventional PSD-95/discs-large/ZO-1 homology (PDZ) binding modes for nonclass II PDZ ligands. J Biol Chem. 2014;289:25327-40.

[74] Lee HJ, Zheng JJ. PDZ domains and their binding partners: structure, specificity, and modification. Cell Commun Signal. 2010;8:8.

[75] Gianni S, Walma T, Arcovito A, Calosci N, Bellelli A, Engström A, et al. Demonstration of long-range interactions in a PDZ domain by NMR, kinetics, and protein engineering. Structure. 2006;14:1801-9.

[76] Lockless SW, Ranganathan R. Evolutionarily conserved pathways of energetic connectivity in protein families. Science. 1999;286:295-9.

[77] Kong Y, Karplus M. Signaling pathways of PDZ2 domain: a molecular dynamics interaction correlation analysis. Proteins. 2009;74:145-54.

[78] Ota N, Agard DA. Intramolecular signaling pathways revealed by modeling anisotropic thermal diffusion. J Mol Biol. 2005;351:345-54.

[79] Amacher JF, Cushing PR, Bahl CD, Beck T, Madden DR. Stereochemical determinants of C-terminal specificity in PDZ peptide-binding domains: a novel contribution of the carboxylate-binding loop. J Biol Chem. 2013;288:5114-26.

[80] Murciano-Calles J, McLaughlin ME, Erijman A, Hooda Y, Chakravorty N, Martinez JC, et al. Alteration of the C-terminal ligand specificity of the erbin PDZ domain by allosteric mutational effects. J Mol Biol. 2014;426:3500-8.

[81] Walma T, Spronk CAEM, Tessari M, Aelen J, Schepens J, Hendriks W, et al. Structure, dynamics and binding characteristics of the second PDZ domain of PTP-BL. Journal of molecular biology. 2002;316:1101-10.

[82] Kuszewski J, Gronenborn AM, Clore GM. Improvements and extensions in the conformational database potential for the refinement of NMR and X-ray structures of proteins and nucleic acids. Journal of magnetic resonance (San Diego, Calif : 1997). 1997;125:171-7.

[83] Laskowski RA, Swindells MB. LigPlot+: multiple ligand-protein interaction diagrams for drug discovery. J Chem Inf Model. 2011;51:2778-86.

[84] van den Berk LC, Landi E, Harmsen E, Dente L, Hendriks WJ. Redox-regulated affinity of the third PDZ domain in the phosphotyrosine phosphatase PTP-BL for cysteine-containing target peptides. FEBS Journal. 2005;272:3306–3316.

[85] van den Berk LC, Landi E, Walma T, Vuister GW, Dente L, Hendriks W.J. An allosteric intramolecular PDZ-PDZ interaction modulates PTP-BL PDZ2 binding specificity. Biochemistry. 2007;46:13629-37.

Table 1: NMR statistics of the final structural ensembles of apo-PDZ3 and the PDZ3/PRK2 complex.

Structure calculation (XPLOR-NIH)	**apo-PDZ3**	**PDZ3/PRK2 complex**
Experimental restraints		
Distance restraints		
Total	**1291**	**1170**
Short-range	**783**	**779**
Medium	**178**	**129**
Long-range	**330**	**246**
Inter-molecular	**0**	**14**
Dihedral angle restraints (φ,ψ)	**184**	**178**
Structural statistics of the final 20 lowest-energy structures		
RMSD [Å]		
Backbone	**0.36 +/- 0.06**	**0.51 +/- 0.09**
Heavy atoms	**0.98 +/- 0.13**	**1.16 +/- 0.17**
rmsd range: **apo-PDZ3:**	*14-20,29-31,46-51,56-72,98-104*	
PDZ3/PRK2 complex:	*15-20,29-32,46-52,63-77,96-103*	
Final energies [kcal mol^{-1}]		
E_{Total}	**102.14**	**105.52**
E_{NOE}	**7.91**	**8.27**
E_{ANGL}	**80.67**	**84.50**
E_{BOND}	**2.02**	**1.96**
E_{DIHE}	**0.18**	**0.08**
E_{IMPR}	**9.70**	**9.74**
E_{VDW}	**2.61**	**2.03**

Restraint violations		
NOE distances violated > 0.5 Å	**0**	**0**
Dihedral angles violated > 5°	**0**	**0**
RMSD from idealised geometry (WHATCHECK)		
Bond lengths [Å]	**0.010**	**0.010**
Bond angles [°]	**1.602**	**1.611**
Ramachandran statistics (PROCHECK-NMR) [%]		
Favoured regions	**68.7**	**70.4**
Additional allowed regions	**29.5**	**26.7**
Generously allowed regions	**1.8**	**2.3**
Disallowed regions	**0.1**	**0.5**

Figures and Figure Captions:

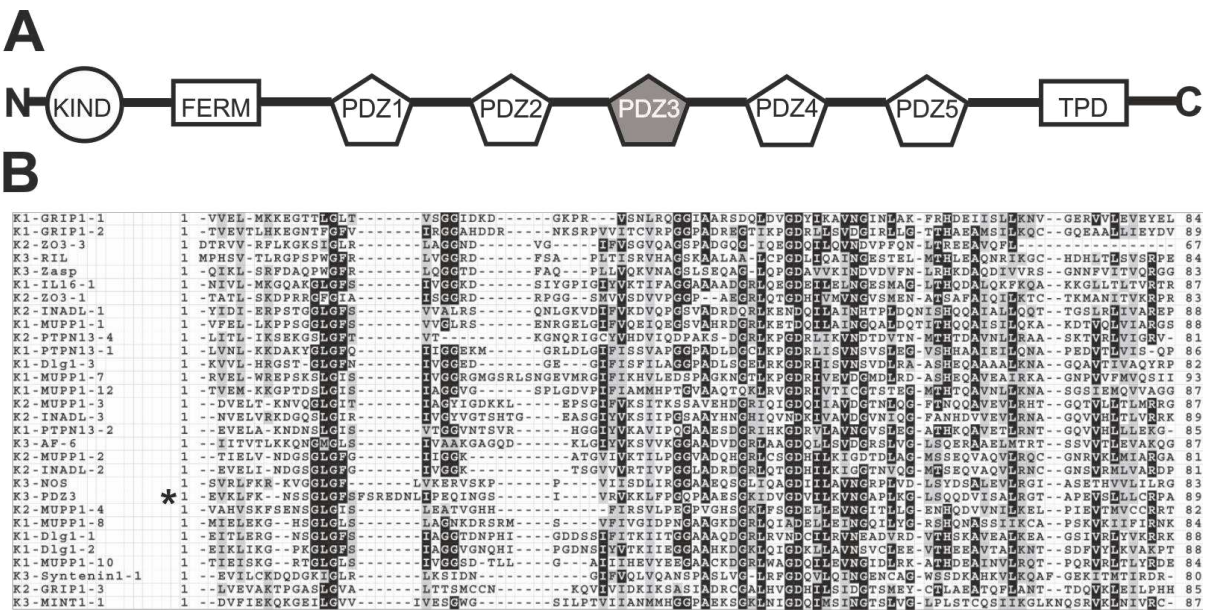

Fig. 1: (A) The modular organisation of murine PTPN13 (UNIPROT accession number Q64512) comprises a KIND domain (residues 3-190) at its amino-terminus (N), followed by a FERM domain (residues 565-865), five PDZ domains (PDZ1: residues 1084-1170; PDZ2: residues 1357-1442; PDZ3: residues 1491-1579; PDZ4: residues 1764-1845; PDZ5: residues 1857-1942), and a carboxy-terminal (C) protein tyrosine phosphatase domain (TPD: residues 2180-2434). **(B)** Sequence alignment of 30 different PDZ domains from all three classes. The coding region of the PDZ3 domain construct from from PTPN13 used in this study comprises amino acid residues 1475 to 1588 (highlighted with an asterisk).

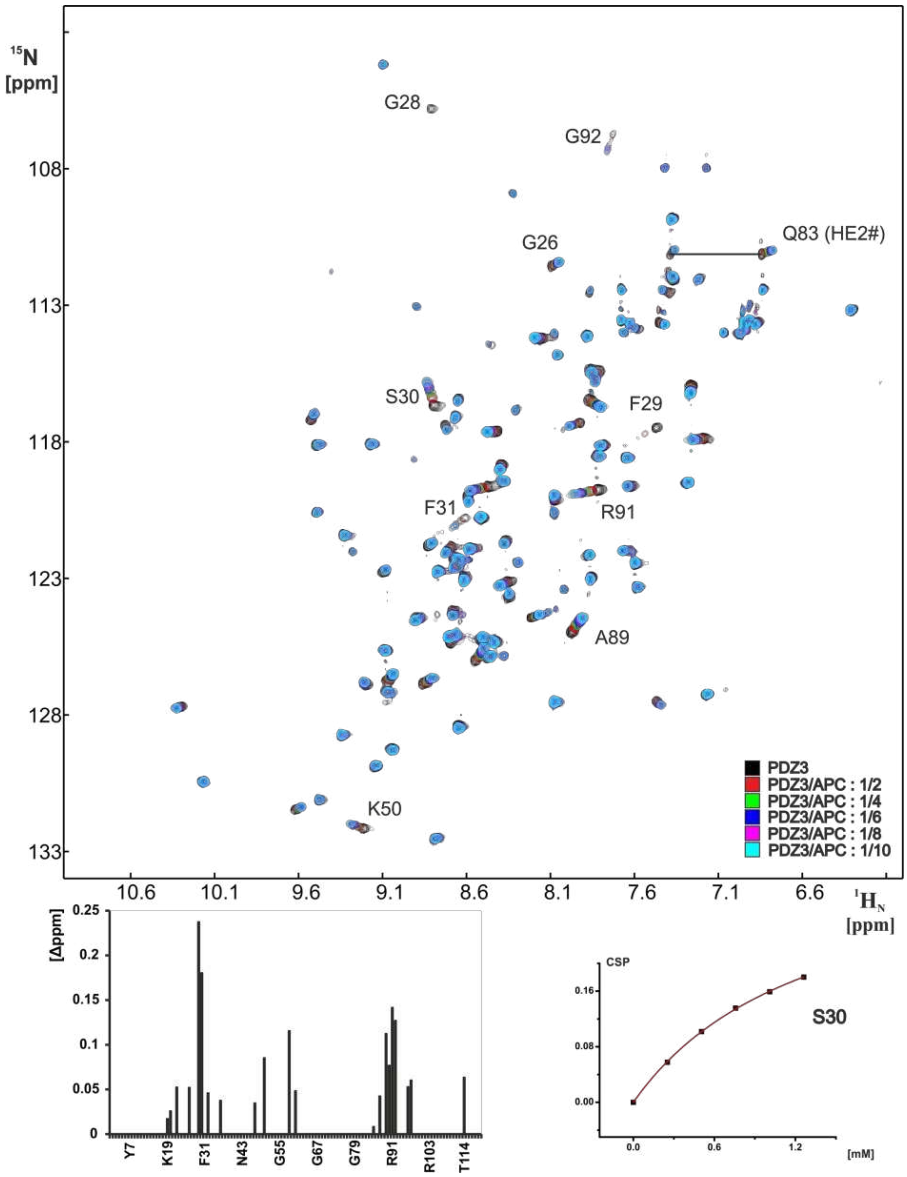

Fig. 2: In the upper part, a 2D ^{1}H-^{15}N-HSQC of the PDZ3/APC complex at different molar ratios given as an insert, 600 MHz, and 298 K is shown. Residue specific assignments of backbone ^{1}H and ^{15}N frequencies are indicated. Signals connected by horizontal lines correspond to side chain amide groups of asparagine and glutamine residues. The plot of the chemical shift dispersion *versus* the amino acid sequence is shown in the lower left corner. The lower right corner displays the curve fitting of amino acid S30 for the PDZ3/APC titration.

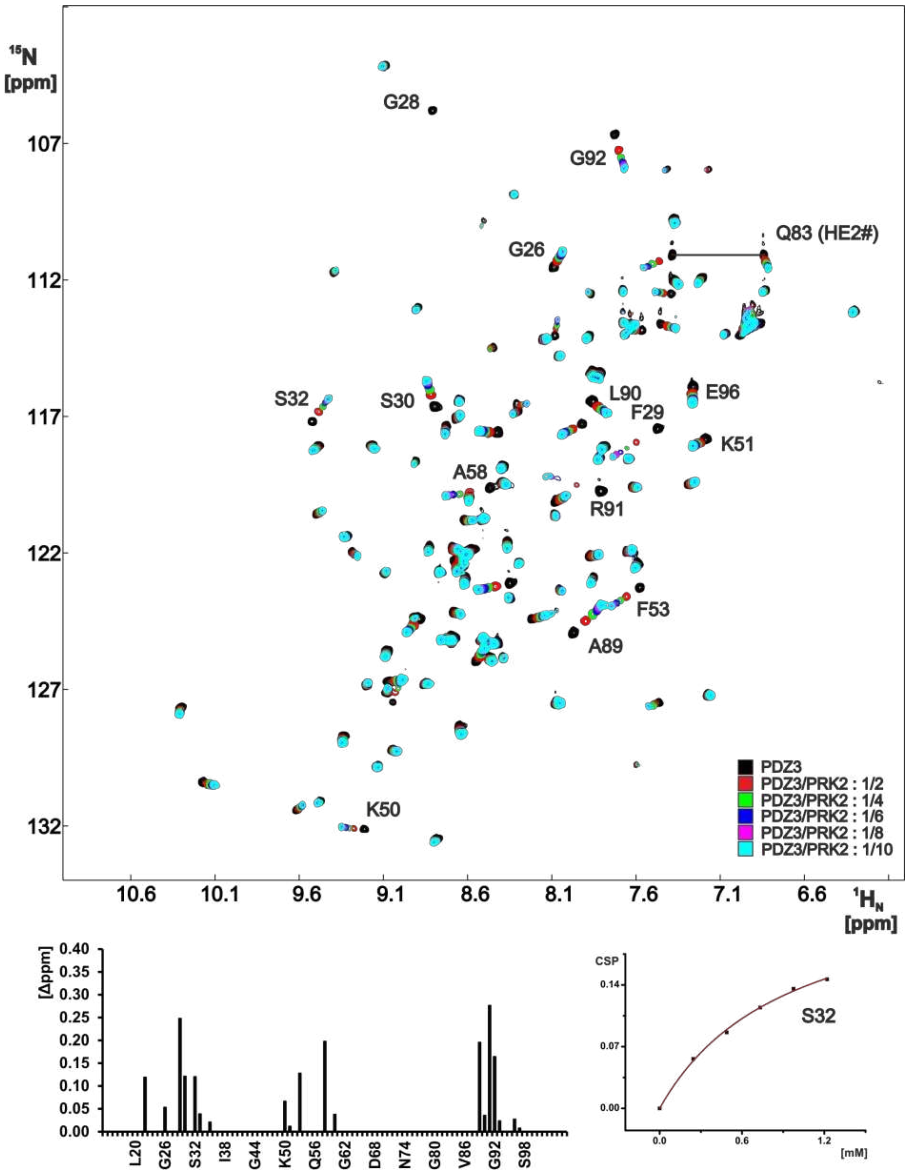

Fig. 3: In the upper part, a 2D ^{1}H-^{15}N-HSQC spectra of the PDZ3/PRK2 complex at different molar ratios given as an insert, 600 MHz, and 298 K is shown. Residue specific assignments of backbone ^{1}H and ^{15}N frequencies are indicated. Signals connected by horizontal lines correspond to side chain amide groups of asparagine and glutamine residues. The plot of the chemical shift dispersion *versus* the amino acid sequence is shown in the lower left corner. The lower right corner displays the curve fitting of amino acid S32 for the PDZ3/PRK2 titration.

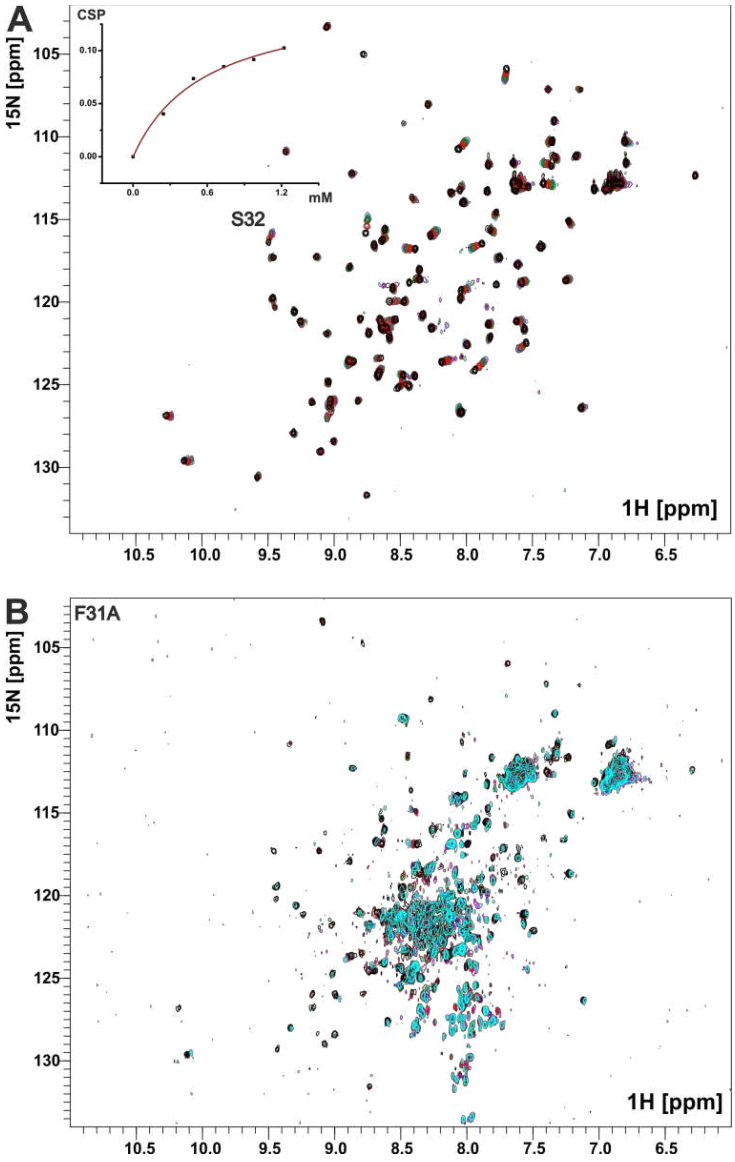

Fig. 4: (A) 2D ^{1}H-^{15}N-HSQC spectra of wildtype PDZ3 titrated with a PRK2 mutant peptide C0V recorded at 700 MHz and 298K. The insert displays the curve fitting of amino acid S32 for the PDZ3/PRK2C0V titration. The colour coding of spectra is the same as in Fig. 2 and 3. **(B)** 2D ^{1}H-^{15}N-HSQC spectra of PDZ3 F31A titrated with a PRK2 mutant peptide C0V recorded at 700 MHz and 298K. Again, the colour coding of spectra is the same as in Fig. 2 and 3.

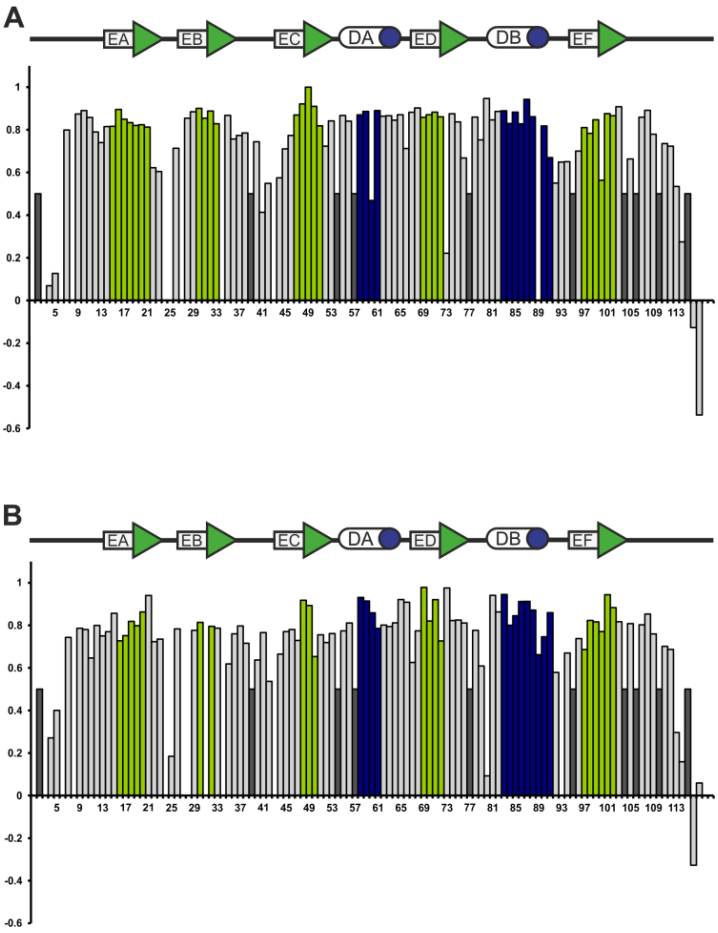

Fig. 5 (A) Plot of the heteronuclear steady-state $^{15}N\{^{1}H\}$-NOE values *versus* residue number for apo-PDZ3 sample. The secondary structure elements are colored as follows: α-helices are highlighted in blue and β sheets in green. **(B)** Plot of the heteronuclear steady-state $^{15}N\{^{1}H\}$-NOE values *versus* residue number for the PDZ3/PRK2 complex. Residues supposed to be flexible exhibit $^{15}N\{^{1}H\}$-NOE values below 0.6. The secondary structure elements are colored as follows: α-helices are highlighted in blue and β sheets in green (EA: T15-F21; EB: F29-R33; EC: I46-L52; ED: D68-V73; EF: E96-C102; DA: P57-S61; DB: Q83-R91). Proline residues are depicted in black.

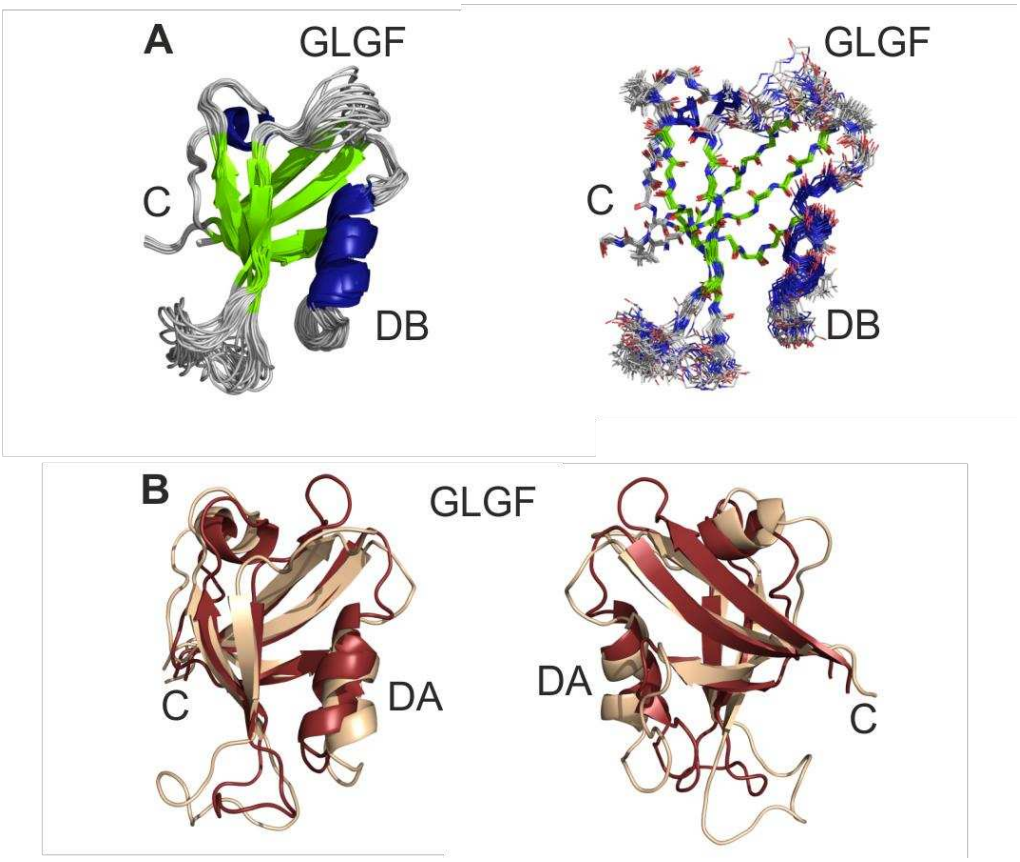

Fig. 6. (A) Ribbon representation of the Xplor-NIH structural ensemble calculated for apo-PDZ3 of PTPN13 generated with PyMOL (www.pymol.org). The left column depicts the apo-PDZ3 domain of PTPN13 in a ribbon representation. In right column, a line representation of the structure in the same orientation is shown. The high precision of the structural ensemble is clearly visible. For the rmsd values refer to Table 1. The secondary structure elements are colored as follows: α-helices are highlighted in blue and β sheets in green. The orientation of the structural ensemble is such that the PDZ binding interface is shown with EB-β-sheet located on the left hand side and the DB-α-helix on the right hand side. Both, the unstructured amino- and carboxy-terminus are not shown for clarity. This figure was generated using PyMOL (www.pymol.org). **(B)** Superposition of the apo-PDZ3 (shown in sandy colour) domain from PTPN13 with its PDZ2 domain (PDB-Code: 1GM1, shown in

red). The orientation between the left and right orientation differs by a rotation of 90º to the left. The overall rmsd is 2.3 Å. This figure was generated using PyMOL (www.pymol.org).

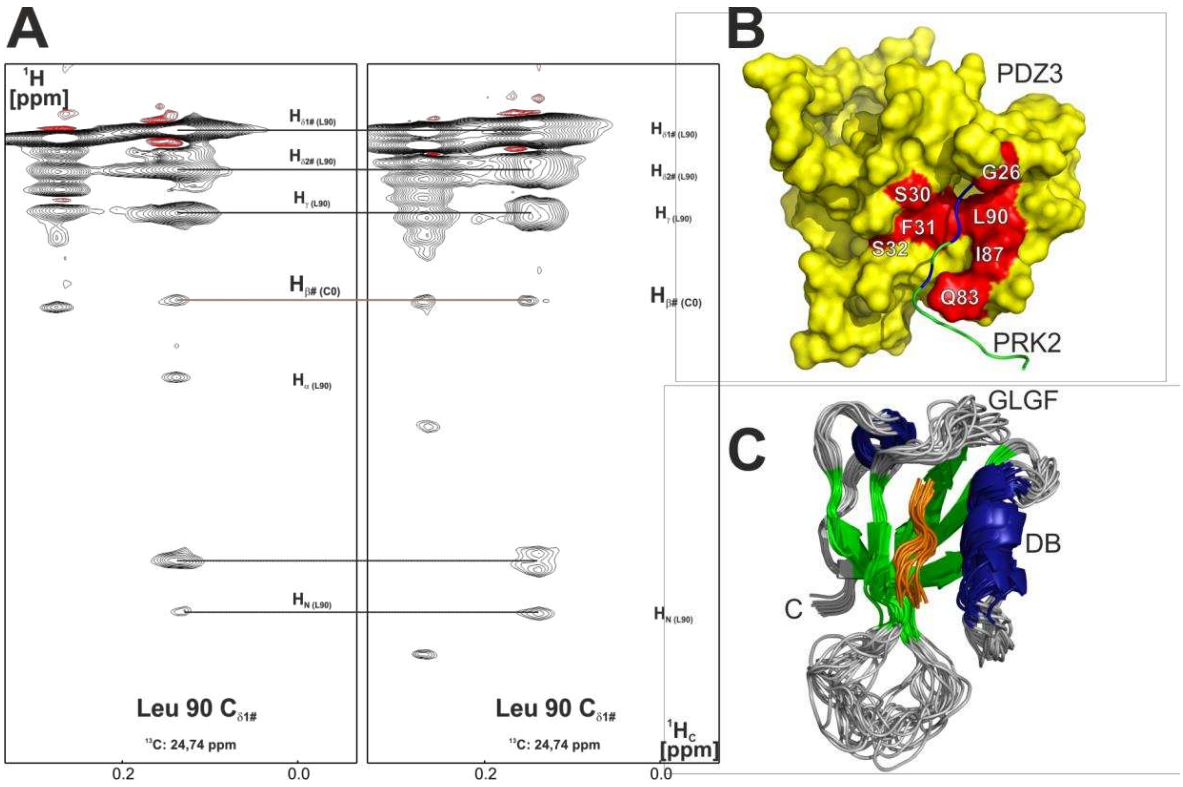

Fig. 7: (A) Strip plot of a ^{1}H-^{13}C NOESY-HSQC spectrum with (left panel) and without (right panel) ^{13}C decoupling in the indirect dimension. A representative intermolecular NOE between $H_{\delta 1\#}$ of L90 from ^{15}N, ^{13}C isotopically-enriched PDZ3 and $H_{\beta\#}$ of C0 from PRK2 is highlighted by an orange horizontal line. The intermolecular NOE does not experience any splitting due to the natural abundance of ^{13}C in the PRK2 peptide (right panel). **(B)** Surface representation of the PDZ3/PRK2 complex. The PDZ3 surface is in shown in yellow. The PRK2 peptide is depicted as a line in green. Residues of PDZ3 for which intermolecular NOEs could be detected are highlighted in red and labelled (G26, S30-S32, Q83, I87, and L90). Residues of PRK2 for which intermolecular NOEs could be identified are highlighted in blue (C0, W-1, D-2, I-4). **(C)** Ribbon representation of all three structural ensembles calculated for PDZ3 of PTPN13 in complex with a PRK2-derived carboxy-terminal peptide. The PDZ3 domain of PTPN13 is shown in ribbon representation. The high precision of the structural ensemble calculated using

Xplor-NIH is clearly visible. The secondary structure elements are colored as follows: α-helices are highlighted in blue and β sheets in green. The orientation of the structural ensemble is such that the PDZ binding interface is shown with EB-β-sheet located on the left hand side and the DB-α-helix on the rind hand side. Both, the unstructured amino- and carboxy-terminus have been omitted for clarity. The five structured amino acids located at the carboxy-terminus of the PRK2 peptide are colored in orange. Figs. 7B and 7C were generated using PyMOL (www.pymol.org).

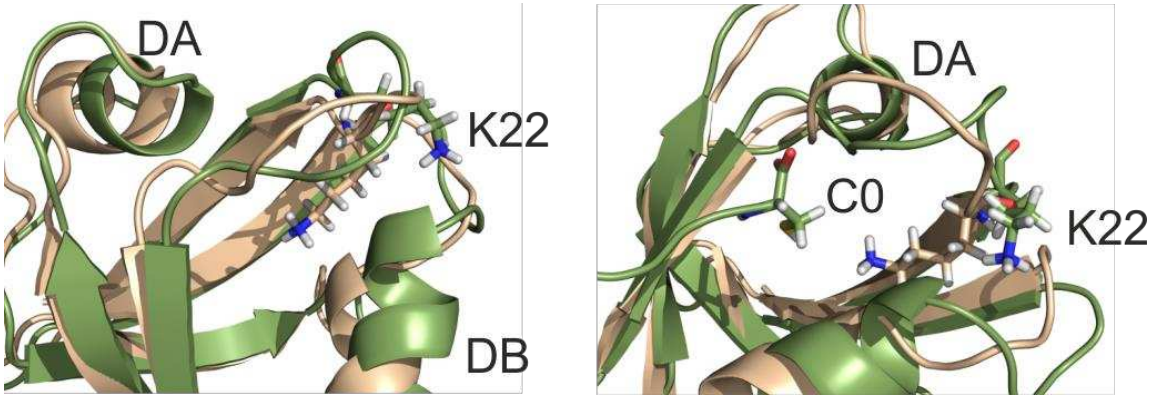

Fig. 8: Detailed ribbon representation of the peptide binding cleft of apo-PDZ3 (shown in sandy colour) and in complex with the PRK2 peptide (shown in green). K22 of PDZ3 and C0 of PRK2 are shown in ball-and-stick representation. On the left hand side, a direct view onto the binding pocket is shown. On the right hand side, the PDZ3 domain is rotated about 90° to the left in order to reveal the steric demand of the carboxy-terminal C0 of the PRK2 peptide as well as the orientation of the K22 side chain. Upon interaction with the PRK2 carboxy-terminus, the K22 side chain of the PDZ3 located at the rear of the empty binding pocket partly flips out. This figure was generated using PyMOL (www.pymol.org).

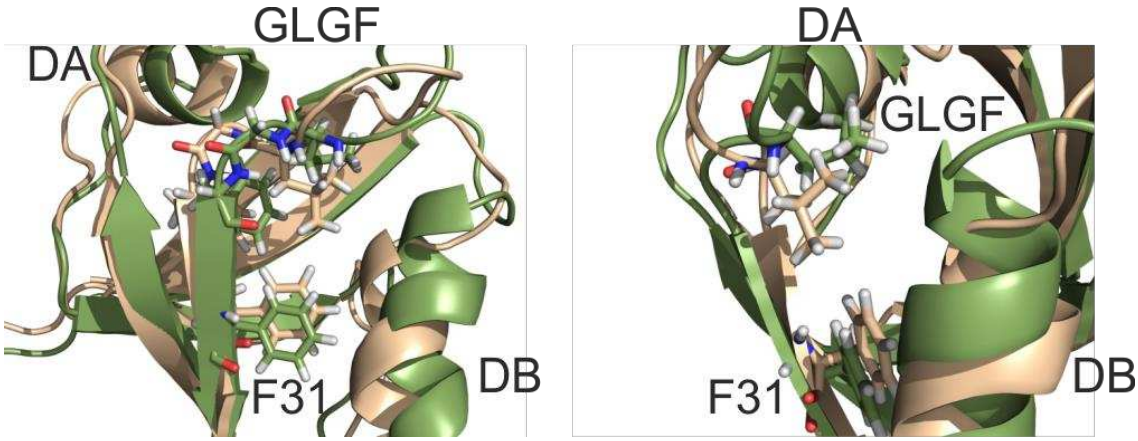

Fig. 9: Orientation of the F31 side chain. This figure was generated using PyMOL (www.pymol.org).

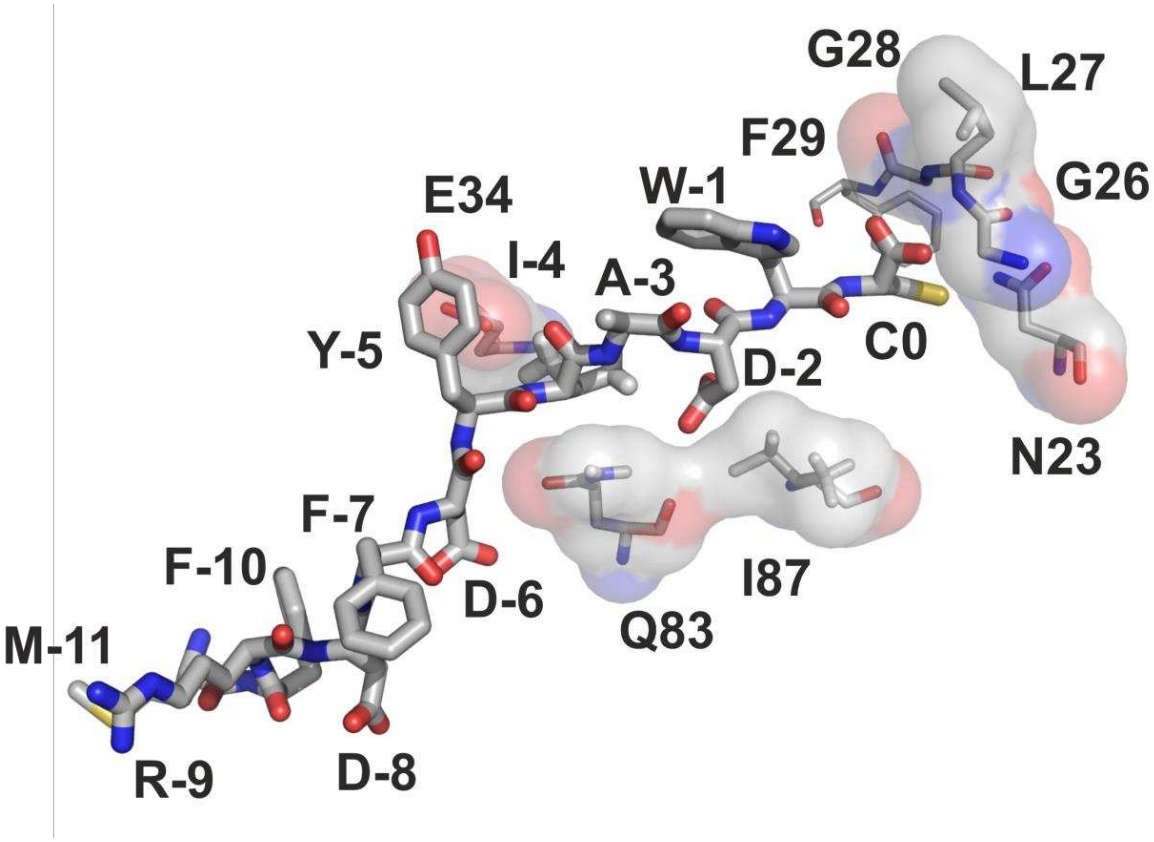

Fig. 10: Molecular recognition of the PRK2-derived dodecapeptide MFRDFDYYIADWC (shown as sticks) by PDZ3 from PTPN13. The charge distribution is shown for residues of PDZ3 (shown in sticks) that contact the PRK2 peptide. This figure was created using LigPlot^{+} [83] and PyMOL (www.pymol.org).